



Study in support effect of $\text{In}_2\text{O}_3/\text{MO}_x$ ($M = \text{Al}, \text{Si}, \text{Zr}$) catalysts for dehydrogenation of propane in the presence of CO_2

Miao Chen^{a,b,*}, Jia-Ling Wu^a, Yong-Mei Liu^a, Yong Cao^{a,**}, Li Guo^b, He-Yong He^a, Kang-Nian Fan^a

^a Shanghai Key Laboratory of Molecular Catalysis and Innovative Materials, Department of Chemistry, Fudan University, Shanghai 200433, PR China

^b Zhejiang Chemical Industry Research Institute, Hangzhou 310023, PR China

ARTICLE INFO

Article history:

Received 31 March 2011

Received in revised form 13 July 2011

Accepted 13 August 2011

Available online 19 August 2011

Keywords:

Indium oxide
Dehydrogenation
Propane
Carbon dioxide
Support effect

ABSTRACT

Two series of binary $\text{In}_2\text{O}_3/\text{MO}_x$ ($M = \text{Al}, \text{Zr}, \text{Si}$) catalysts with low (3 wt%) and high (10 wt%) In_2O_3 loadings were prepared via an incipient wetness impregnation method. The support effect has been investigated in detail by testing the propane dehydrogenation (PDH) reaction both in the presence and absence of CO_2 . Physico-chemical properties including surface composition, redox and acidic/basic properties of the supported In_2O_3 were characterized by X-ray diffraction, X-ray photoelectron spectroscopy, H_2 temperature-programmed reduction, NH_3 and CO_2 temperature-programmed desorption, respectively. It was demonstrated that a higher population of the specific highly dispersed In_2O_3 species on support is favorable for propylene production, and the maximum propylene yield was achieved with the high-loading $\text{In}_2\text{O}_3/\text{Al}_2\text{O}_3$. Properties including high In_2O_3 dispersion and balanced acidic/basic properties, rendering synergism between dehydrogenation and reverse water gas shift, are essential for achieving high catalytic performance of PDH.

© 2011 Elsevier B.V. All rights reserved.

1. Introduction

Light alkenes such as propylene are important building blocks in a myriad of (petro)chemical applications thus, their demand is high [1,2]. A great deal of attention has been paid to the so-called *on-purpose* propylene production technologies, such as propane dehydrogenation (PDH) [3,4], due to their potential to make-up the shortfall of propylene supply left by conventional crackers where propylene is produced as a byproduct of ethylene. However, due to the thermodynamic constrains of PDH reaction, high reaction temperature is frequently used, which inevitably leads to severe coke formation as well as undesired thermal cracking to lighter alkanes [5,6]. Hence extra hydrogen addition in the gas feed and repeated regeneration are indispensable procedures implemented, making this process energy and capital intensive. An attractive alternative to this approach is the oxidative dehydrogenation (ODH) of propane by molecular oxygen, which allows significantly lower reaction temperature and effective inhibition of coke deposition [7]. Nevertheless, significant loss of propylene selectivity due to

deep oxidation to carbon oxides is inevitably accompanied, existing as the main drawback of this process [1].

To circumvent this problem, carbon dioxide (CO_2), one of the most important green-house gases, has been proposed to be a promising candidate as milder oxidant replacing oxygen in activation of light alkanes, including coupling of methane, dehydrogenation (DH) of ethylbenzene, *iso*-propylbenzene, propane, or *iso*-butane [8]. In the DH reaction, CO_2 is also expected to serve as a medium for supplying heat for the endothermic dehydrogenation reaction, as a diluent for enhancing the equilibrium conversion of light alkanes and as an agent for the removal of coke formed on the catalyst [9]. On the other hand, contrarily to what is traditionally believed, CO_2 is not inert in the oxidation reaction. Oxygen species produced by its dissociation can modify the oxidation state of the surface atoms of the catalysts and can directly participate in the oxidation of the hydrocarbon [10,11]. Besides, taking into account the environmental concerns, CO_2 , one of the major green-house gases, accounts for the fast global warming tendency in the past decades. In this context, CO_2 recycling by the PDH technique, not only produces useful chemicals but also helps alleviate environmental pressure for excessive burning of fossil fuels, seemingly attractive from both economic and ecological perspective [12].

To date, in the field of PDH by CO_2 , Cr_2O_3 -, V_2O_5 - and Ga_2O_3 -based materials are the most frequently reported catalytic systems. For the Cr_2O_3 - and V_2O_5 -based catalysts, the proposed one-step pathway is followed, in agreement with the Mars–Van Krevelen mechanism [13,14]. The Ga_2O_3 -based catalysts is proposed to obey

* Corresponding author at: Zhejiang Chemical Industry Research Institute, ODS Substitution Research Department, Tianmushan Road No. 387, Hangzhou, Zhejiang 310023, PR China. Tel.: +86 571 85223785.

** Corresponding author.

E-mail addresses: chenmiao@sinochem.com (M. Chen), yongcao@fudan.edu.cn (Y. Cao).

a two-step pathway mechanism, which is a simple dehydrogenation step coupled with a subsequent reverse water gas shift (RWGS) reaction [15,16]. However, fast deactivation presents as a common problem troubling all the above-mentioned catalyst systems, ascribed to either exhaustion of active lattice oxygen atoms or coke deposition. Thus catalysts with prolonged lifetime are still highly desired. Along this line, we have recently demonstrated that $\text{In}_2\text{O}_3\text{-Al}_2\text{O}_3$ nanocomposite synthesized via alcoholic coprecipitation was highly active and stable a new catalyst in the PDH with CO_2 [17,18]. An interesting feature of the In–Al–O catalyzed PDH reaction is the unique bifunctional character of the indium component in the $\text{In}_2\text{O}_3\text{-Al}_2\text{O}_3$ materials, where a well balance of the metallic In species active and the bulk In_2O_3 phase is found to be indispensable for an efficient CO_2 -mediated propane dehydrogenation over the $\text{In}_2\text{O}_3\text{-Al}_2\text{O}_3$ system.

In addition to the specific active phases, the choice of the support, conventionally thought to play important role in the dispersion and electronic properties of the dispersed active species, is able to tune further the catalytic performance of a given catalyst [1]. It is also suggested that acid–base properties of supports strongly affect the selectivity to propylene [2]. Hence, it is necessary to gain further insight into the support effect for the In-based catalysts. To this end, in the present study, the support effect for In-based catalysts has been studied, and Al_2O_3 , ZrO_2 and SiO_2 were selected as three supports, taking into account their differentiated surface properties in terms of affinity to In_2O_3 and relative acid/base strength. For each support, both low and high In-loading samples were synthesized. Detailed correlation of characterization results and PDH activities performed reveals the abundance of highly dispersed indium-species and acid–base properties are two key parameters that determine the high PDH performance for the In-based catalysts.

2. Experimental

2.1. Catalyst preparation

The samples were prepared by incipient wetness impregnation using the appropriate amounts of $\text{In}(\text{NO}_3)_3 \cdot 5\text{H}_2\text{O}$ from Aldrich (99.99%) in order to obtain two different indium oxide loadings for each support, one series of samples with loadings around 3 wt% (hereafter named In(3)/M or low loading samples) and the second one with loadings around 10 wt% (hereafter named In(10)/M or high loading samples). The support SiO_2 was purchased from Degussa (Aerosil 380) and was pre-calcined at 873 K for 6 h. $\gamma\text{-Al}_2\text{O}_3$ and ZrO_2 were prepared by adding an aqueous solution of ammonia (concentrated aqueous ammonia:water = 50:50 in volume) into 0.2 M ZrOCl_2 ($\text{ZrOCl}_2 \cdot 8\text{H}_2\text{O}$, Aldrich 99.9%) and 0.2 M $\text{Al}(\text{NO}_3)_3$ ($\text{Al}(\text{NO}_3)_3 \cdot 9\text{H}_2\text{O}$, Fluka 99.9%) solutions, respectively, followed by aging overnight, filtering, washing, drying at 393 K for 6 h, and calcination at 873 K for 6 h. After impregnation, the samples were dried at 393 K overnight and calcined at 873 K in air for 6 h. Bulk In_2O_3 was prepared by calcination of indium nitrate at 873 K for 6 h after drying at 393 K overnight.

2.2. Catalyst characterization

The BET specific surface areas of the samples were determined by adsorption–desorption of nitrogen at liquid nitrogen temperature, using a Micromeritics TriStar 3000 equipment. Sample degassing was carried out at 300 °C prior to acquiring the adsorption isotherm. The X-ray powder diffraction (XRD) of the catalysts was carried out on a Bruker D8 Advance X-ray diffractometer using nickel filtered $\text{Cu K}\alpha$ radiation at 40 kV and 20 mA, 0.02° step size, and 0.2 s step time. The acidic and basic properties

of each catalyst were characterized by temperature-programmed desorption (TPD) of NH_3 and CO_2 , respectively. In a typical experiment for TPD studies, about 200 mg of the oven-dried sample (dried at 383 K overnight) was placed in a U-shaped quartz sample tube. NH_3 (or CO_2) was saturated at 413 K after pre-treatment at 773 K in a He stream. The NH_3 (or CO_2) desorbed was determined by gas chromatography at temperatures from 413 to 873 K at a ramp rate of 10 K min^{-1} and subsequently maintained at 873 K for 30 min.

The XPS spectra were recorded under vacuum ($<10^{-6}$ Pa) on a Perkin-Elmer PHI 5000C ESCA system equipped with a dual X-ray source using an $\text{Mg K}\alpha$ ($h\nu = 1253.6 \text{ eV}$) anode and a hemispheric energy analyzer. The binding energies (BE) were referenced to the C 1s peak of contaminant carbon at 284.6 eV with an uncertainty of $\pm 0.2 \text{ eV}$. Elemental analysis was performed using ion-coupled plasma (ICP) atomic emission spectroscopy on a Thermo Electron IRIS Intrepid II XSP spectrometer. Temperature-programmed reduction (TPR) results were obtained on a homemade apparatus loaded with 20 mg of catalyst. The samples were pretreated in flowing nitrogen at 773 K for 1 h. After cooled to room temperature, the samples were subsequently contacted with an H_2/Ar mixture (H_2/Ar molar ratio of 5/95 and a total flow of 40 mL min^{-1}) and heated at a rate of 5 K min^{-1} , to a final temperature of 1073 K. The H_2 consumption was monitored by an on-line TCD detector. Thermal gravimetric analysis (TGA) was conducted on a Perkin-Elmer TGA-7 apparatus to determine the amount of coke deposited on the catalyst after the reaction. Twenty milligrams of sample was heated from room temperature to 873 K at a heating rate of 10 K min^{-1} in flowing air.

2.3. Catalytic activity tests

Catalytic tests were performed in a fixed-bed microreactor at ambient pressure. The catalyst load was 200 mg, and it was activated at 873 K in N_2 (BOC 99.99%) for 2 h prior to the reaction. For nonoxidative PDH, the gas reactant contained 2.5 vol% propane (BOC 99.5%) and a balance of nitrogen. For PDH by carbon dioxide, the gas reactant contained 2.5 vol% propane, 10 vol% carbon dioxide (BOC 99.99%), and a balance of nitrogen. The total flow rate of gas reactant was 10 mL min^{-1} . The feed and the reaction products were analyzed on-line by online gas chromatograph (Type GC-122, Shanghai). Permanent gases (CO , CO_2) and water (H_2O) were separated using a TDX-01 column connected to a TCD detector and other reaction products were analyzed employing a Porapak Q column connected to a FID detector. Blank runs show that under the experimental conditions used in this work the thermal dehydrogenation could be neglected. During reaction no aromatic products were detected by GC, and all carbon balances closed within 92–95%.

2.4. Temperature-programmed reaction of CO_2 with H_2

A temperature-programmed $\text{CO}_2\text{-H}_2$ test was carried out to investigate the activity of the supported In_2O_3 catalysts for the RWGS reaction. The measurements were performed in a flow microreactor system. Prior to the experiment, a sample (100 mg) was outgassed in a flow of pure helium at 873 K for 30 min. Subsequently, the microreactor was cooled down to about 443 K. Reaction was performed using $\text{CO}_2/\text{H}_2/\text{He}$ gas mixture with the ratio of 1:1:4 and total flow rate of 12 mL min^{-1} . The experiment was carried out with a linear heating rate of 10 K min^{-1} up to the final temperature of 973 K. The reactants and all possible products of reaction were continuously monitored by the QMS detector (Balzers OmniStar). The signal of the helium line served as the internal standard to compensate fluctuations of the operating pressure.

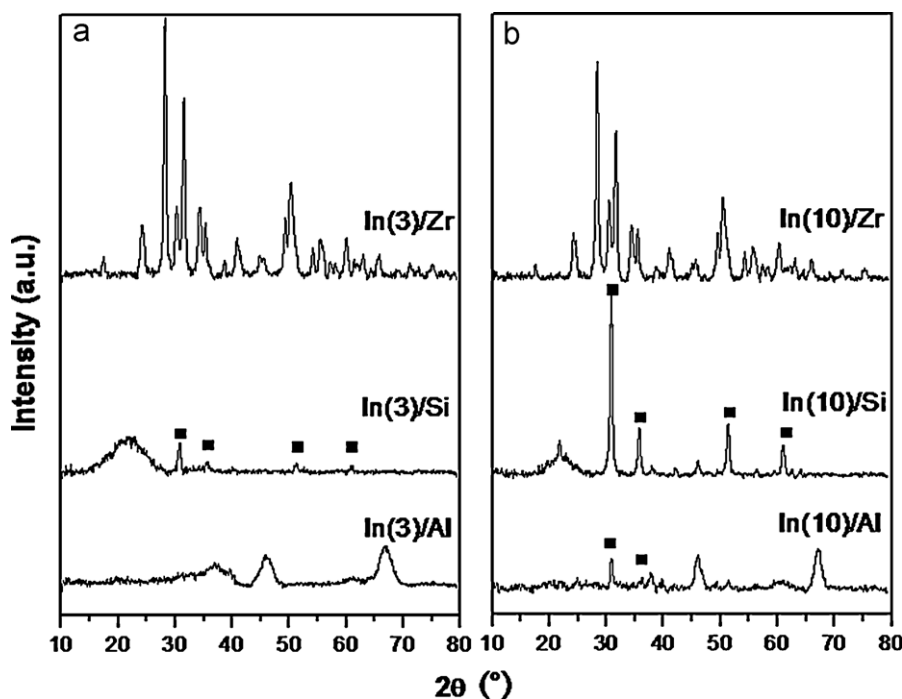


Fig. 1. XRD profiles for the two series of as-synthesized supported In_2O_3 samples: (a) 3 wt%; (b) 10 wt%; (■) indicates characteristic peaks of $c\text{-In}_2\text{O}_3$.

3. Results

3.1. XRD results

The XRD profiles of both high and low loading samples as synthesized are shown in Fig. 1. The diffraction patterns for samples In/Zr containing In_2O_3 up to 10% are characteristic of bare zirconia support (monoclinic zirconia (JCPDS card 37-1484) in majority together with a small fraction of tetragonal zirconia (JCPDS card 17-923)). In the case of In/Al, no diffraction lines other than those of the $\gamma\text{-Al}_2\text{O}_3$ support (JCPDS card 10-425) are observed for the low loading sample, while in In(10)/Al diffraction patterns characteristic of the cubic structure of In_2O_3 (JCPDS card 6-0416) have been identified, despite their relatively weak intensities. In sharp contrast to the above two series, for the silica supported catalysts, even in the low indium loading sample signals regarding crystallized indium oxide species have readily formed. And further enhancement in In_2O_3 loading up to 10% results in well defined diffraction peaks of $c\text{-In}_2\text{O}_3$. It should be pointed out that in all supported indium oxide samples, the intensities of the diffraction peaks and their positions for the different supported indium oxide samples are very similar to bulk indium oxide, indicating that the support does not have a significant influence on the crystallization of indium oxide, and in particular does not favor the crystallization in a special plane. The widths at half-height (FWHM) of the diffraction peaks are related to the size of the crystal phases; with respect to this criterion, the dispersion at same indium loading levels is obviously the poorest for In/Si.

3.2. Redox properties and XPS studies

The reducibility of indium species in supported In_2O_3 catalysts was investigated by TPR experiments and the profiles are given in Fig. 2. All the samples exhibit two reduction features during TPR in the temperature range of 473–773 K (peak α) and 773–1073 K (peak β) respectively. Park et al. reported similar observations in their study of supported $\text{In}_2\text{O}_3/\text{Al}_2\text{O}_3$ catalysts for the selective catalytic reduction of NO_x and also compared the reduction behavior

of indium oxide at different loadings [19]. Perdigon-Melon et al. suggested that the two characteristic reduction peaks for indium species were generally attributed to the reduction of indium oxide particles ($\text{In}^{3+} \rightarrow \text{In}^0$) of different sizes, i.e. the peak α corresponds to the reduction of highly dispersed indium oxide species while peak β to bulk In_2O_3 [20]. To determine the amount of each indium oxide species, all hydrogen consumption with respect to α and β peaks, respectively were calculated, and collected in Table 1. From these data, it is clear that by raising In_2O_3 content from 3% up to 10% over the same support, the hydrogen consumption (β) increases more rapidly than that of α , suggesting a favored creation of aggregated In_2O_3 particles at higher indium surface concentrations. This observation is fully consistent with the properties of $\text{In}_2\text{O}_3/\text{Al}_2\text{O}_3$ catalysts reported by Park et al. [19]. As far as the support effect is concerned, note that the amount of highly dispersed In_2O_3 represented by H_2 consumption (α) varied distinctly among different In/M series at identical In-loadings, ranked as follows: In/Al > In/Zr \gg In/Si. This result, together with the XRD measurements, suggests an apparently higher dispersion of surface In_2O_3 species for over In/Al and In/Zr in contrast to In/Si.

XPS gives an idea on both the oxidation state and concentration of indium on the surface of the sample. For all fresh samples used in the present work, only one oxidation state was found, with In $3d_{5/2}$ binding energy between 444.5 and 444.8 eV, characteristic of In(III). Loading of In_2O_3 over ZrO_2 , Al_2O_3 and SiO_2 seems to have little influence on BE of Al $2p_{3/2}$, Zr $3d_{5/2}$ and Si $2p$ of the supports (Table 2). To gain further insight into the chemical state of the supported indium species during reduction procedure and the possible influence of CO_2 exposure upon the in situ-created metallic indium, XPS studies on In(3)/Al subjected to various atmospheric treatments were performed (see Fig. 3). In the case of the fresh In(3)/Al sample (Fig. 3a), only bands assigned to In(III) species were observed. After reduction treatment at 773 K (Fig. 3b), an additional feature signaling the formation of metallic In^0 (BE In $3d_{5/2} = 443.5$ eV) species was shown [17]. The In^0 accounted for 36.5% of the overall indium atoms based on deconvolution analysis, in agreement with that (33%, in Table 1) of its likely precursor (highly dispersed In_2O_3) calculated based on TPR data, implying all

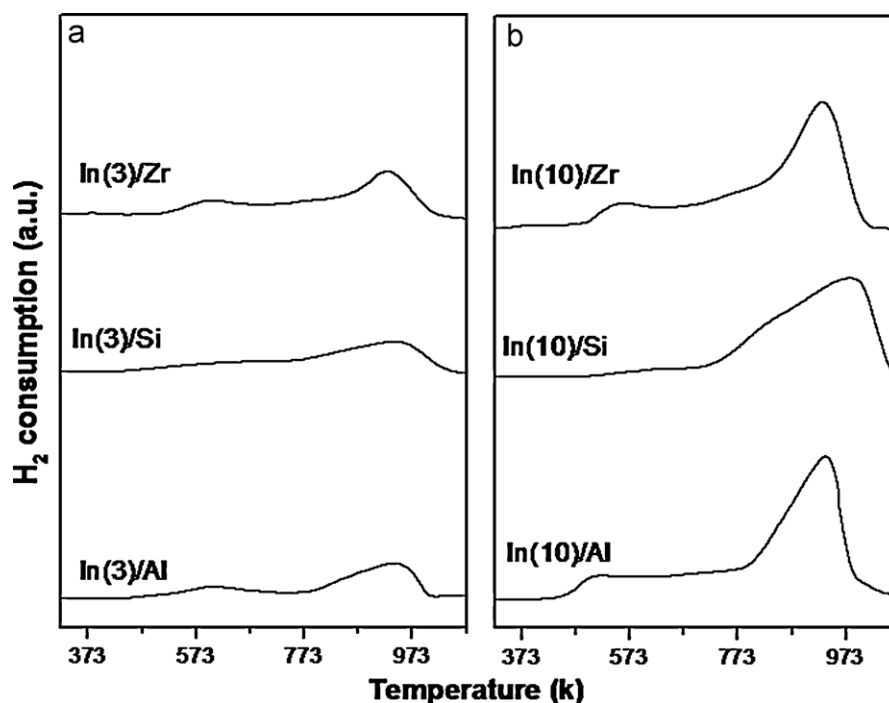


Fig. 2. TPR profiles for the two series of supported In_2O_3 catalysts: (a) 3 wt%; (b) 10 wt%.

Table 1
Physicochemical properties and characterization results of the supported In_2O_3 samples.

Sample	Loading wt% In_2O_3	S_{BET} ($\text{m}^2 \text{g}^{-1}$)	In/M molar ratio		H_2 consumption (μmol)		Percentage of In_2O_3 (a) ^e (%)	Coke ^f (%)
			Bulk ^a	Surface ^b	α^c	β^d		
In_2O_3	100	23	–	–	0	216	0	1.1
In(3)/Al	3	112	0.011	0.01	2.1	4.3	33	(1.5) 2.2
In(10)/Al	9.9	105	0.036	0.031	3.8	15.7	19	(2.9) 4.4
In(3)/Zr	3	34	0.026	0.024	1.9	4.5	30	(1.8) 2.7
In(10)/Zr	9.4	30	0.084	0.073	3.1	15	17	(3.7) 5.6
In(3)/Si	2.7	264	0.012	0.007	1	4.5	18	(0.9) 1.3
In(10)/Si	9.6	259	0.042	0.015	0.7	17.9	3.7	(1.4) 1.9

^a The bulk In/Al molar ratio calculated from the ICP data.

^b The surface In/Al molar ratio based on XPS analysis.

^c The hydrogen consumption during 423–773 K calculated from the TPR results.

^d The hydrogen consumption during 773–1073 K calculated from the TPR results.

^e The percentage of In_2O_3 reduced during 423–773 K in TPR from the total amount of In_2O_3 reduced during the whole temperature range.

^f The value inside and outside the bracket are the amount of coke deposit of the catalysts tested in the absence and presence of CO_2 for 8 h, respectively.

the existing In^0 derived largely from the highly dispersed In_2O_3 . Further exposure to CO_2 at 873 K was also carried out, led to no spectral variation (Fig. 3c), suggesting the preformed metallic In^0 cannot be re-oxidized by CO_2 under reaction conditions (Fig. 3d), in line with the weak oxidant nature of CO_2 [8].

Table 2
Summary of XPS studies.

Sample	BE (eV)			
	In 3d _{5/2}	Al 2p _{3/2}	Zr 3d _{5/2}	Si 2p
In_2O_3	444.7	–	–	–
Al_2O_3	–	74.7	–	–
In(3)/Al	444.6	74.8	–	–
In(10)/Al	444.5	74.8	–	–
ZrO_2	–	–	183.2	–
In(3)/Zr	444.6	–	183.2	–
In(10)/Zr	444.6	–	183.1	–
SiO_2	–	–	–	103.9
In(3)/Si	444.5	–	–	104
In(10)/Si	444.6	–	–	104.1

3.3. Surface acid/base properties

The surface acidity of the supported In_2O_3 catalysts with both high and low loadings was measured by NH_3 -TPD, and the quantified results are provided in Table 3. Dumesic and co-workers have discussed the generation of acid sites when one oxide is deposited onto another to form a surface-phase oxide [21]. Thus, it is interesting to study the acidity of the indium oxide loaded on different supports. The acidic strength distribution by NH_3 -TPD is described in two temperature regions (i.e. 443–773 and 773–873 K), which point to acid sites with weak and medium strength, respectively. The number and density of acidic sites were both calculated according to their corresponding peak intensities as well as BET surface areas, expressed in terms of $\text{mmol g}_{\text{cat}}^{-1}$ and $\mu\text{mol m}_{\text{cat}}^{-2}$, respectively. For each support, increasing In-loading from 3% to 10% all results in a pronounced decrease in total acidity, which was associated with the less acidic site amount for indium oxide in contrast to those for the bare supports. Similar observation was obtained by Gervasini et al. in their in-depth study of a series of supported In_2O_3 catalysts based on characterization of ammonia adsorption calorimetry

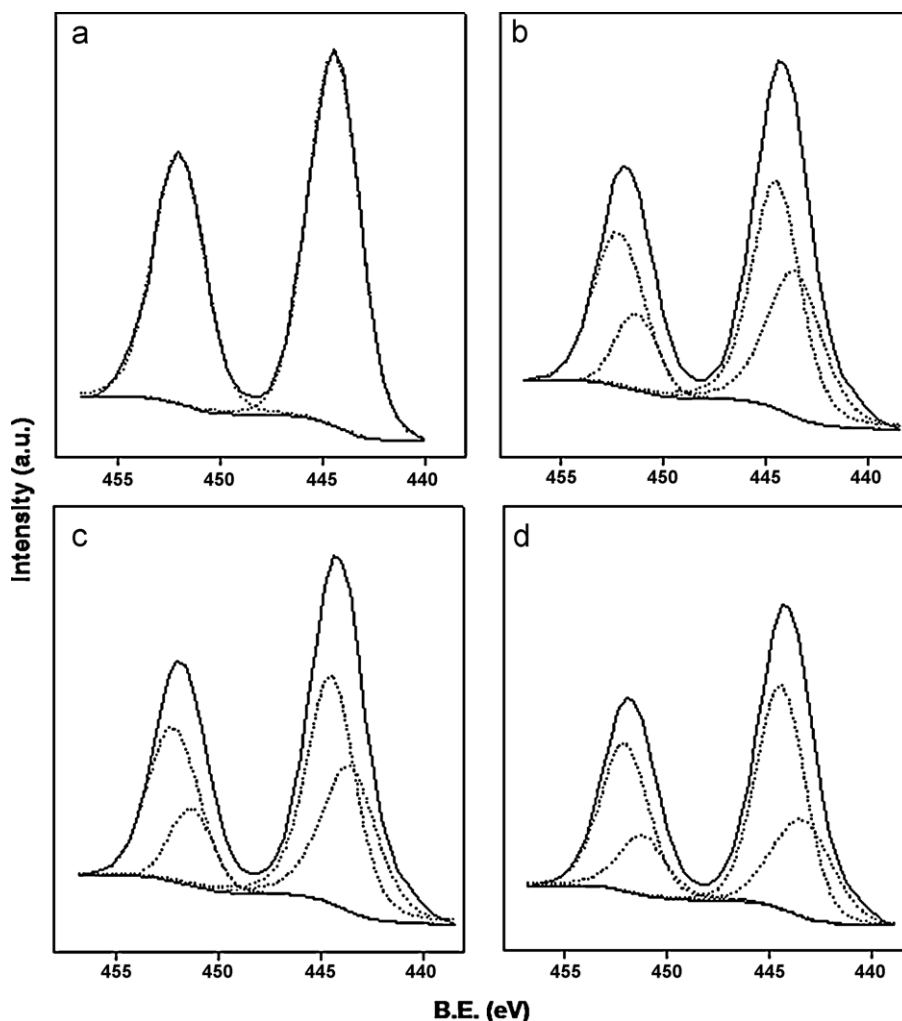


Fig. 3. XPS results of the In(3)/Al catalyst under different atmospheric treatments: (a) fresh In(3)/Al; (b) In(3)/Al pre-reduced by H₂/Ar at 773 K for 1 h; (c) In(3)/Al pre-reduced by H₂/Ar at 773 K for 1 h followed by exposure to a CO₂ stream (10 mL min⁻¹) at 873 K for 1 h; (d) In(3)/Al reacted for 3 h on stream at 873 K in the presence of CO₂ (reaction conditions: $P(\text{C}_3\text{H}_8) = 2.5 \text{ kPa}$; $P(\text{CO}_2) = 10 \text{ kPa}$; $P(\text{N}_2) = 87.5 \text{ kPa}$; total flow rate: 10 mL min⁻¹).

[22]. Taking the support effect into account, at identical indium loading levels, the zirconia supported samples exhibit the highest overall acidic site densities (10–12 $\mu\text{mol m}_{\text{cat}}^{-2}$), followed by alumina loaded ones (5–6 $\mu\text{mol m}_{\text{cat}}^{-2}$), and those for silica supported samples amount to only 1.1–1.5 $\mu\text{mol m}_{\text{cat}}^{-2}$, dramatically lower than the former two series.

The basicity measurements of all the supported In₂O₃ catalysts were carried out by CO₂-TPD. Again, two asymmetric des-

orption peaks were observed at: 443–753 K and 753–873 K, which define weak and medium basic sites, respectively. Detailed information with respect to desorption peak T_{max} values, quantified basic site amount and density (expressed in terms of $\text{mmol g}_{\text{cat}}^{-1}$ and $\mu\text{mol m}_{\text{cat}}^{-2}$, respectively) were all collected in Table 4. From these results, it is obvious that the specific basic site density of the catalysts decreases in the order of In(10)/Zr > In(3)/Zr > In(10)/Al > In(3)/Al > In(10)/Si > In(3)/Si,

Table 3
Summary of NH₃-TPD measurements.

Catalyst	Peak temperature (K)		NH ₃ desorbed					
	α	β	α (443–773 K)		β (773–873 K)		Total	
			$\text{mmol g}_{\text{cat}}^{-1}$	$\mu\text{mol m}_{\text{cat}}^{-2}$	$\text{mmol g}_{\text{cat}}^{-1}$	$\mu\text{mol m}_{\text{cat}}^{-2}$	$\text{mmol g}_{\text{cat}}^{-1}$	$\mu\text{mol m}_{\text{cat}}^{-2}$
In ₂ O ₃	523	873	0.05	2.2	0.07	3.0	0.12	5.2
Al ₂ O ₃	573	873	0.64	2.7	0.31	2.0	0.95	4.7
In(3)/Al	583	873	0.47	4.2	0.21	1.8	0.68	6.0
In(10)/Al	633	873	0.35	3.3	0.19	1.8	0.54	5.1
ZrO ₂	563	873	0.28	7.6	0.23	6.2	0.51	13.8
In(3)/Zr	569	873	0.23	6.7	0.17	5.0	0.40	11.7
In(10)/Zr	583	873	0.20	6.7	0.12	4.0	0.32	10.7
SiO ₂	607	873	0.19	0.60	0.25	0.80	0.44	1.4
In(3)/Si	613	873	0.16	0.60	0.23	0.90	0.39	1.5
In(10)/Si	613	873	0.07	0.30	0.11	0.40	0.18	0.70

Table 4
Summary of CO₂-TPD measurements.

Catalyst	Peak temperature (K)		CO ₂ desorbed					
	α	β	α (443–753 K)		β (753–873 K)		Total	
			mmol g _{cat} ⁻¹	$\mu\text{mol m}_{\text{cat}}^{-2}$	mmol g _{cat} ⁻¹	$\mu\text{mol m}_{\text{cat}}^{-2}$	mmol g _{cat} ⁻¹	$\mu\text{mol m}_{\text{cat}}^{-2}$
In ₂ O ₃	530	873	0.08	3.5	0.14	6.1	0.22	9.6
Al ₂ O ₃	570	873	0.34	1.5	0.15	0.64	0.49	2.1
In(3)/Al	547	873	0.08	0.71	0.2	1.8	0.28	2.5
In(10)/Al	569	873	0.24	2.3	0.12	1.1	0.36	3.4
ZrO ₂	567	873	0.16	4.3	0.10	2.6	0.26	6.9
In(3)/Zr	560	873	0.14	4.1	0.10	2.9	0.24	7
In(10)/Zr	550	873	0.13	4.3	0.10	3.3	0.23	7.6
SiO ₂	558	873	0.02	0.07	0.04	0.15	0.06	0.22
In(3)/Si	565	873	0.02	0.07	0.04	0.15	0.06	0.22
In(10)/Si	590	873	0.03	0.12	0.09	0.35	0.12	0.47

confirming that the select of support has a significant impact on the surface basicity of the supported In₂O₃ materials. It is noteworthy that the basic site density for In/Zr is 2.2–2.8 and 16–34 times higher than those for In/Al and In/Si, respectively, suggesting a dramatically higher basicity for In/Zr compared with the other two counterpart series. Through comparison of the results at different indium loadings, one can easily discover that an increase in In₂O₃ content for all three series leads to an appreciable enhancement in basicity, contrary to their observed trend in acid properties. This feature is resulted from the more basic character of In₂O₃ in contrast to the three bare supports.

3.4. Dehydrogenation activities

The dehydrogenation of propane to propylene over the high indium loading supported materials along with the unsupported In₂O₃ in the presence of CO₂ was investigated at 873 K. The major product formed in the reaction is propylene, and the minor products are ethane, ethylene, and methane. The results, shown in Fig. 4, point to a marked support effect on the catalytic performance of the supported samples. Unsupported In₂O₃ demonstrated low propane conversion of <10% and deactivated fast within 5 h, which is fully in line with its inferior dehydrogenation activities as reported by Nakagawa et al. [23]. It is noteworthy that In(10)/Si closely

resembled bulk In₂O₃ in catalytic behavior and deactivated in 8 h. In contrast, remarkably higher propane conversions were observed for In(10)/Al (20–24%) and In(10)/Zr (25–28%). Another interesting finding is that, during 0–3 h, In(10)/Al and In(10)/Zr exhibited relatively low conversions of propane as well as extremely poor selectivities to propylene. In our previous study, such unique induction period has been attributed to the in situ creation of In⁰ species generated from the well-dispersed In₂O₃ under reductive atmosphere, and this specific In⁰ species is confirmed as the intrinsic active center for dehydrogenation [17]. Maximum propane conversions over In(10)/Zr and In(10)/Al were achieved at 3 h, followed by gradual deactivation at a moderate rate due to coke formation. The coke amounts for all the samples reacted for 8 h have been determined by TGA (Table 1). The coke amount for In(10)/Al reacted for 3 h was further studied, exhibiting a weight loss of 2.1%. Through comparison of In(10)/Zr with In(10)/Al, superior “initial” propane conversion (27.9% at 3 h) was observed for In(10)/Zr in contrast to 23.6% for In(10)/Al. However, if calculated in terms of propylene yield, due to a higher selectivity to propylene (84%) for In(10)/Al than In(10)/Zr (63.4%), In(10)/Al appears to be the optimal sample obtaining the maximum propylene yield (19.8%). The lower selectivity for In(10)/Zr was ascribed to more severe cracking which gave rise to the production of methane and ethylene.

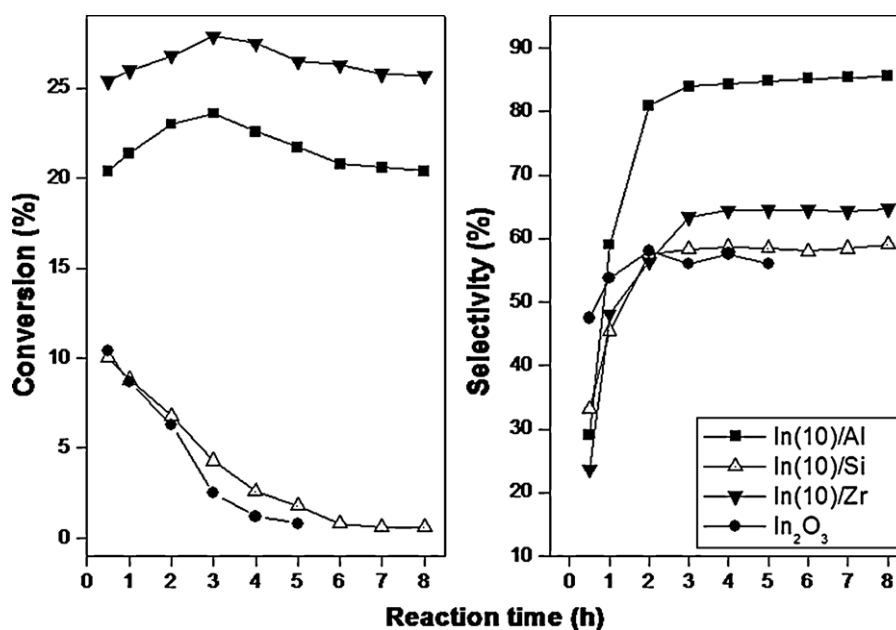


Fig. 4. Conversion of propane and selectivity to propylene for the 10 wt% supported In₂O₃ samples in the presence of CO₂. Reaction conditions: catalyst weight: 200 mg; $P(\text{C}_3\text{H}_8) = 2.5 \text{ kPa}$; $P(\text{CO}_2) = 10 \text{ kPa}$; $P(\text{N}_2) = 87.5 \text{ kPa}$; total flow rate: 10 mL min^{-1} .

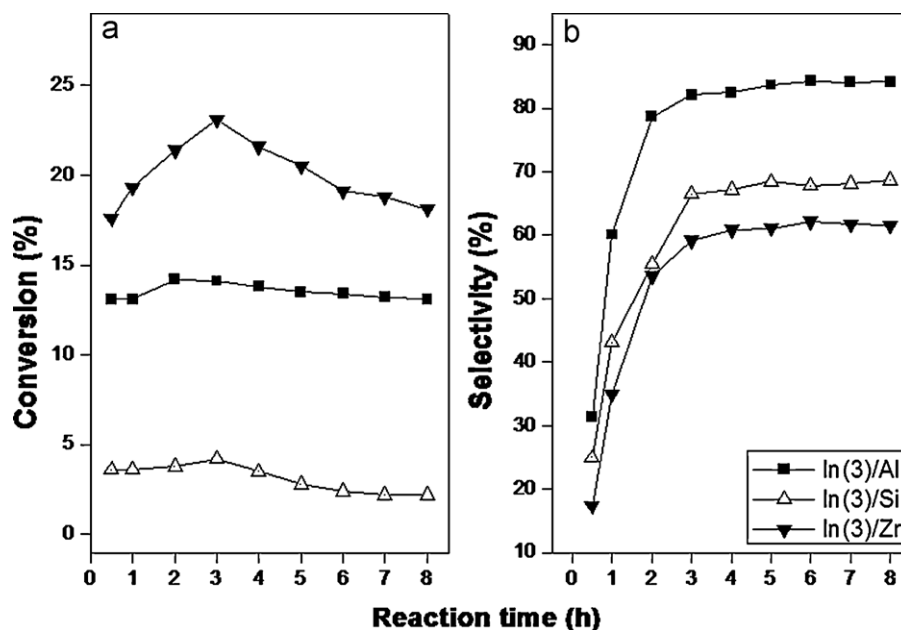


Fig. 5. Conversion of propane and selectivity to propylene for the 3 wt% supported In_2O_3 samples in the presence of CO_2 . Reaction conditions: catalyst weight: 200 mg; $P(\text{C}_3\text{H}_8) = 2.5 \text{ kPa}$; $P(\text{CO}_2) = 10 \text{ kPa}$; $P(\text{N}_2) = 87.5 \text{ kPa}$; total flow rate: 10 mL min^{-1} .

Dehydrogenation of propane in the presence of CO_2 was also performed over the low In_2O_3 loading samples, and their conversions of propane and selectivities to propylene as a function of the reaction time have been depicted in Fig. 5. The characteristic 3-h induction period was shown for all three samples including In(3)/Si. In contrast, recall that no feature of induction period was observed for the high loading In/Si sample (Fig. 4). This is because the indium species over SiO_2 at 10% In-loading comprises predominantly crystallized In_2O_3 as evidenced by TPR, allowing In(10)/Si to resemble bulk In_2O_3 largely in catalytic behavior;

whereas In(3)/Si consists of well-dispersed In_2O_3 at considerably higher percentage that results in this unique feature. In contrast to In/Si, for In(3)/Zr and In(3)/Al, similar trend in activity development and selectivities to those of the high loading samples were observed, but with decreased propane conversions by 5–10%. Moreover, analogous to those for the high loading samples, the “initial” steady yields of propane at 3 h for the low-loading catalysts decreased in the same order: In(3)/Al > In(3)/Zr > In(3)/Si, further suggesting a marked support effect for the supported In_2O_3 catalysts.

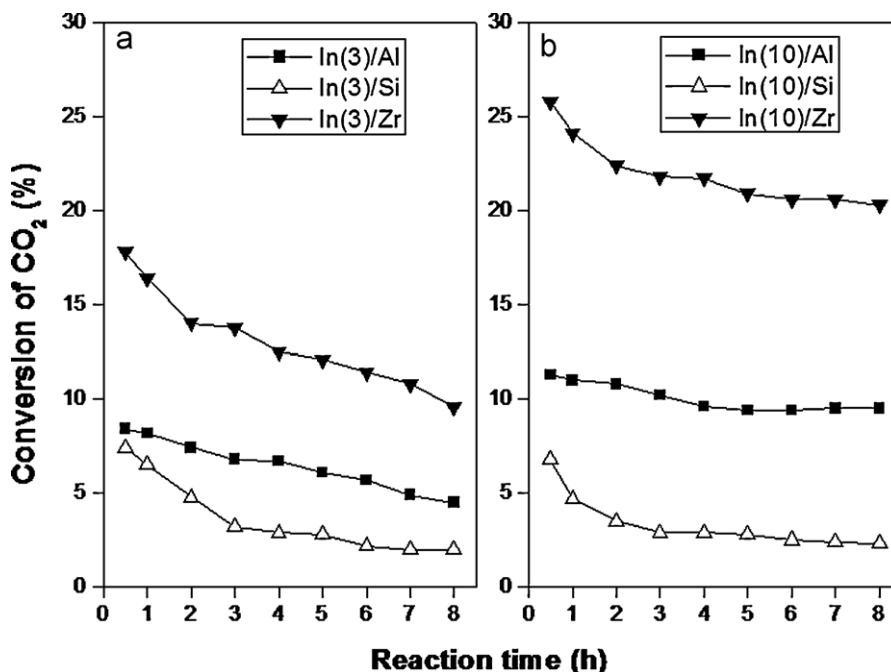


Fig. 6. Conversion of carbon dioxide for the two series of supported In_2O_3 samples: (a) 3 wt%; (b) 10 wt%. Reaction conditions: catalyst weight: 200 mg; $P(\text{C}_3\text{H}_8) = 2.5 \text{ kPa}$; $P(\text{CO}_2) = 10 \text{ kPa}$; $P(\text{N}_2) = 87.5 \text{ kPa}$; total flow rate: 10 mL min^{-1} .

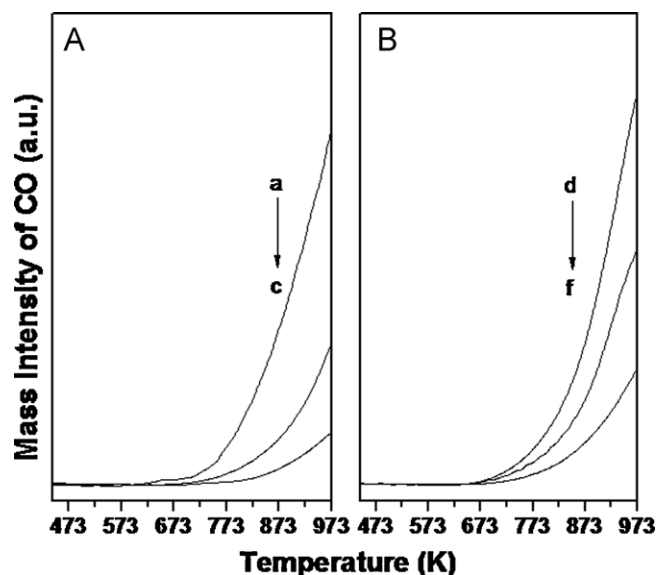


Fig. 7. Temperature-programmed $\text{CO}_2\text{-H}_2$ tests of CO_2 with H_2 for supported In_2O_3 samples: (a) $\text{In}(3)/\text{Zr}$; (b) $\text{In}(3)/\text{Al}$; (c) $\text{In}(3)/\text{Si}$; (d) $\text{In}(10)/\text{Zr}$; (e) $\text{In}(10)/\text{Al}$; (f) $\text{In}(10)/\text{Si}$.

Of further note is the conversion of CO_2 during PDH. As a general trend, over the same support, the CO_2 conversions at high In_2O_3 loadings are apparently higher than those at low loadings (Fig. 6). As far as the support effect is concerned, surprisingly, CO_2 conversions for $\text{In}(10)/\text{Zr}$ (20–26%) are remarkably higher than those for the other two series (i.e. 9–12% for $\text{In}(10)/\text{Al}$ and 2–7% for $\text{In}(10)/\text{Si}$). It is known that higher conversion of CO_2 may facilitate DH via RWGS [8], thus it is interesting to further investigate the activity of RWGS over the supported In_2O_3 catalysts. To this end, temperature-programmed test of $\text{CO}_2\text{-H}_2$ were carried out, and the results were provided in Fig. 7. In the whole reaction temperature range (443–973 K), it is evident that for either 3 wt% (Fig. 7A) or 10 wt% (Fig. 7B) series, the sequence of RWGS activities arrays as

$\text{In}/\text{Zr} > \text{In}/\text{Al} > \text{In}/\text{Si}$, in agreement with those for the conversions of CO_2 and propane during PDH in the presence of CO_2 (Figs. 4–6). Namely the high conversion of CO_2 during PDH for In/Zr could be related to RWGS, which accounts for the promotional effect of CO_2 to PDH.

Given that the CO_2 reactivity varied depends on the support employed, which meanwhile controls the extent to which PDH is facilitated by RWGS, the support effect concluded from the above-mentioned experiments actually reflected a combined result of PDH and RWGS. However, the “pure” support effect on PDH solely still remains unclear. To clarify this point, the PDH in the absence of CO_2 was also conducted. For both high and low loading samples, the characteristic phenomenon of induction period showed again, but lasted for only 2 h (Fig. 8a and b). The sequence of activity at identical indium loadings arrayed as follow: $\text{In}/\text{Al} > \text{In}/\text{Zr} > \text{In}/\text{Si}$. For further analysis, a correlation between active site amount and propane conversion in the absence of CO_2 has been made. In Fig. 8c, a linear relationship of metallic In^0 (active species for PDH [17]) amount represented by H_2 consumption (α) and propane conversion was shown, suggesting the key role of the abundance of active sites in determining the PDH activities. In contrast to those in the presence of CO_2 , conversions of propane were generally lower. Interestingly, note that the sequence for DH activity ($\text{In}/\text{Al} > \text{In}/\text{Zr} > \text{In}/\text{Si}$) differed distinctly in contrast to the original $\text{In}/\text{Zr} > \text{In}/\text{Al} > \text{In}/\text{Si}$ for in the presence of CO_2 . Detailed calculation suggests In/Zr to be with the largest activity discrepancy compared between two atmospheric conditions (by c.a. 16% at 3 h). This feature is coherent with the highest CO_2 conversions in PDH achieved over In/Zr samples (Fig. 6). In addition, comparing the coke amounts of samples reacted for 8 h in the presence and absence of CO_2 , relatively milder coking rate was observed for those in the absence of CO_2 (Table 1).

4. Discussion

It has been established in our previous study that dehydrogenation of propane over In_2O_3 -based catalysts completes within two steps: direct PDH ($\text{C}_3\text{H}_8 \rightarrow \text{C}_3\text{H}_6 + \text{H}_2$) and RWGS ($\text{CO}_2 + \text{H}_2 \rightarrow \text{CO} + \text{H}_2\text{O}$) [17]. Presence of CO_2 can enhance the

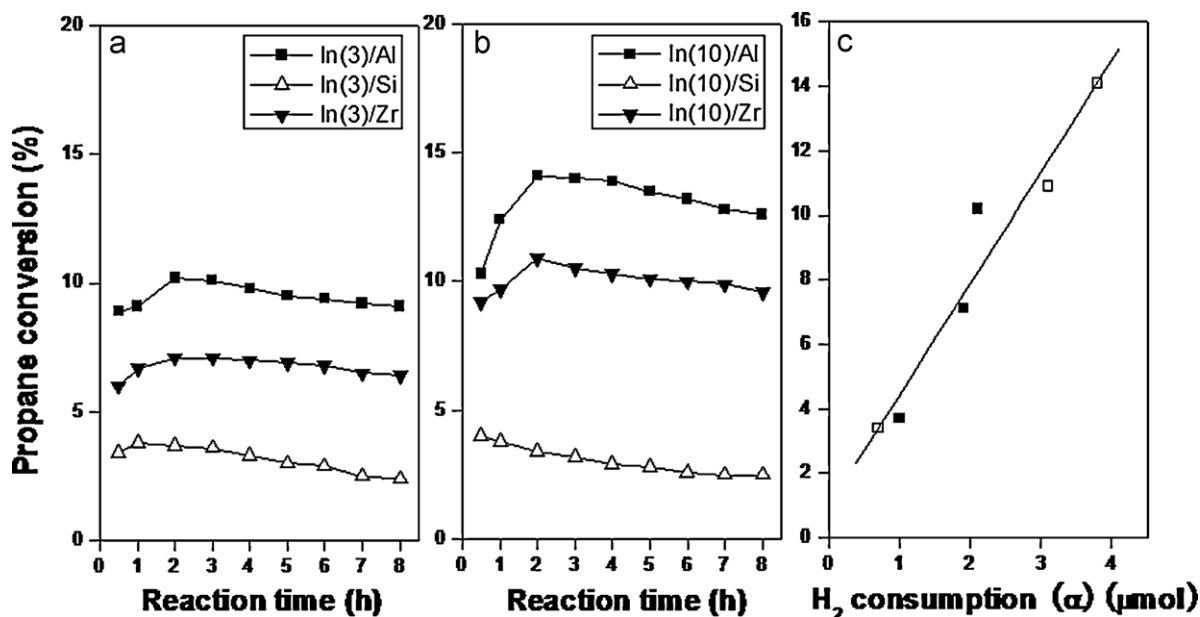


Fig. 8. Conversion of propane in the absence of CO_2 for the two series of supported In_2O_3 samples: (a) 3 wt%; (b) 10 wt%. (c) Relationship between propane conversion at 2 h on stream in the absence of CO_2 and the corresponding hydrogen consumption (α) of the two series of supported In_2O_3 samples: (■) 3 wt%; (□) 10 wt%. Reaction conditions: catalyst weight: 200 mg; $P(\text{C}_3\text{H}_8) = 2.5$ kPa; $P(\text{N}_2) = 97.5$ kPa; reaction temperature: 873 K; total flow rate: 10 mL min^{-1} .

equilibrium conversion of propane by consumption of H₂ via RWGS [8]. The support effects demonstrated in the above experiments actually impact either PDH or RWGS. Among these support effects, dispersion of In₂O₃ could be the most important factor in tuning DH activity, especially during the direct PDH step. In our previous study, metallic In⁰ derived in situ from the highly dispersed In₂O₃ has been proven to be the essential active phase for direct PDH [17]. This conclusion is also applicable for the supported In₂O₃ catalysts, as confirmed by the positive correlation between DH activity and the amount of metallic In⁰ (Fig. 8c). Careful design in select of support which offers In₂O₃ dispersion high can therefore be of key significance as to allowing for abundant precursor of active sites for PDH. Judging from the XRD and TPR results, SiO₂ appears to be poor in dispersing the In₂O₃ aggregate. In this sense, Al₂O₃ and ZrO₂ were shown to be supports certainly more appropriate for loading In₂O₃, in view of their far superior dispersion of In-species, as well as obviously higher PDH results both in the presence and absence of CO₂.

Further considering the surface acid/base properties, as suggested by NH₃/CO₂-TPD results, the acidity/basicity of the supported catalysts depend largely on the properties of the supports. Generally, the total acid/basic site density arrayed as: In/Zr > In/Al > In/Si, fully in line with those of the bare supports. In contrast to bare supports, since bulk In₂O₃ is considered as a basic solid [20], as a general rule, the total acidity of In/M was decreased and the basicity increased by increasing the loading of indium oxide. This fact is consistent with the result by Gervasini et al. [22] on study of supported In₂O₃ over Al₂O₃, TiO₂, SiO₂ and Nb₂O₅. Therefore, appropriate acid/base strength can be achieved by employment of a suitable support and loading level.

As far as correlation between catalytic performance and acid–base properties is concerned, it is known that superior surface basicity favors adsorption and subsequent reaction of acidic molecules (such as CO₂) [24]. In a study by Xu et al. for the supported Ga₂O₃ catalysts for PDH, the lowest RWGS activity for Ga₂O₃/SiO₂ was accounted for by its inferior basicity [12]. In our previous study, bulk In₂O₃ rather than Al₂O₃ was suggested to favor RWGS to a certain extent due to its higher basicity in contrast to Al₂O₃ [17]. In this study, as revealed by CO₂-TPD experiment (Table 4), the basic site density for In/Zr is far superior in contrast to the other two counterpart series, which may well account for its extraordinarily high conversion of CO₂ during RWGS (Fig. 7). Bear in mind further that In/Zr is with the largest discrepancy in conversion of propane compared between two conditions (in the presence/absence of CO₂, see in Figs. 4 and 5). Thus, it can be inferred that, the extraordinarily high surface basic density for In/Zr allows for its highest RWGS activity, which facilitates PDH to a great extent.

Another parameter noteworthy is acidity, since suitable surface acidity is commonly accepted as a crucial factor for achieving high DH activities [2]. In this sense, superior surface acidity for In/Zr and In/Al in contrast to In/Si is another noticeable factor contributing to their higher PDH activities. Nevertheless, it has been also well established that surface acidity too strong usually renders undesired side-reactions, such as cracking and coking etc. [25]. Due to its highest acid site density, cracking is pronounced for In/Zr. Namely, the relatively milder surface acid site density (Table 3) for In/Al in contrast to In/Zr may well account for its apparently higher selectivity to propylene (Figs. 4 and 5). Considering both conversion of propane and selectivity to propylene for PDH in the presence of CO₂, Al₂O₃ seems to be a more appropriate support for loading In₂O₃ in contrast to ZrO₂. Based on the above results, it can be concluded that, in order to achieve selectively high conversion of propane for the supported In₂O₃ samples, well dispersion of In₂O₃ and balanced acid–base properties are two prerequisites indispensable.

5. Conclusions

The dehydrogenation of propane both in the presence and absence of CO₂ were studied over three In-based catalytic systems prepared by dispersing various amounts of In₂O₃ over different supports. Alumina was found to be the most effective support in terms of preparing active and selective dehydrogenation catalysts. Generally, supports that are able to disperse the In₂O₃ aggregates with high In⁰ stabilization in situ could offer active catalytic systems. The better dispersion of In₂O₃ by alumina and zirconia in contrast to silica, confirmed by XRD and TPR studies, perfectly explain their higher activities in dehydrogenation. Correlation of acid/base characterization and activities further revealed a high density of basic sites over In/Zr that accounted for its remarkable promotion of RWGS, which facilitates the PDH. Superior catalytic performance in PDH with CO₂ over alumina supported indium samples were due mainly to a combined effect of high In₂O₃ dispersion and balanced acid/base properties.

Acknowledgments

This work was financially supported by the National Natural Science Foundation of China (20873026 and 21073042), New Century Excellent Talents in the University of China (NCET-09-0305), the National Basic Research Program of China (2009CB623506), and Science & Technology Commission of Shanghai Municipality (08DZ2270500).

References

- [1] R. Grabowski, *Catal. Rev.* 48 (2006) 199–268.
- [2] M.M. Bhasin, J.H. McCain, B.V. Vora, T. Imai, P.R. Pujado, *Appl. Catal. A: Gen.* 221 (2001) 397–419.
- [3] P. Michorczyk, J. Ogonowski, *Appl. Catal. A* 251 (2003) 425–433.
- [4] S. Sugiyama, Y. Hirata, K. Nakagawa, K.I. Sotowa, K. Maehara, Y. Himeno, W. Ninomiya, *J. Catal.* 260 (2008) 157–163.
- [5] O.A. Barias, A. Holmen, E.A. Blekkan, *J. Catal.* 158 (1996) 1–12.
- [6] D. Vitry, J.-L. Dubois, W. Ueda, *J. Mol. Catal. A: Chem.* 220 (2004) 67–76.
- [7] F. Kapteijn, J. Rodriguez-Mirasol, J.A. Moulijn, *Appl. Catal. B: Environ.* 9 (1996) 25–64.
- [8] S.B. Wang, Z.H. Zhu, *Energy Fuels* 18 (2004) 1126–1139.
- [9] L. Liu, H. Li, Y. Zhang, *Catal. Commun.* 8 (2007) 565–570.
- [10] H.Y. Li, Y.H. Yue, C.K. Miao, Z.K. Xie, W.M. Hua, Z. Gao, *Catal. Commun.* 8 (2007) 1317–1322.
- [11] Y. Sakurai, T. Suzuki, N. Ikenaga, T. Suzuki, *Appl. Catal. A: Gen.* 192 (2000) 281–288.
- [12] B.J. Xu, B. Zheng, W.M. Hua, Y.H. Yue, Z. Gao, *J. Catal.* 239 (2006) 470–477.
- [13] H. Shimada, T. Akazawa, N. Ikenaga, T. Suzuki, *Appl. Catal. A: Gen.* 168 (1998) 243–250.
- [14] Y. Wang, Y. Ohishi, T. Shishido, Q.H. Zhang, W. Yang, Q. Guo, H.L. Wan, K. Takehira, *J. Catal.* 220 (2003) 347–357.
- [15] M. Chen, J. Xu, F.Z. Su, Y.M. Liu, Y. Cao, H.Y. He, K.N. Fan, *J. Catal.* 256 (2008) 293–300.
- [16] K. Nakagawa, C. Kajita, K. Okumura, N.-o. Ikenaga, M. Nishitani-Gamo, T. Ando, T. Kobayashi, T. Suzuki, *J. Catal.* 203 (2001) 87–93.
- [17] M. Chen, J. Xu, Y. Cao, H.-Y. He, K.-N. Fan, J.-H. Zhuang, *J. Catal.* 272 (2010) 101–108.
- [18] M. Chen, J. Xu, Y.-M. Liu, Y. Cao, H.-Y. He, J.-H. Zhuang, *Appl. Catal. A: Gen.* 377 (2010) 35–41.
- [19] P.W. Park, C.S. Ragle, C.L. Boyer, M.L. Balmer, M. Engelhard, D. McCready, *J. Catal.* 210 (2002) 97–105.
- [20] J.A. Perdigon-Melon, A. Auroux, *J. Catal.* 234 (2005) 421–430.
- [21] G. Connell, J.A. Dumesic, *J. Catal.* 105 (1987) 285–298.
- [22] A. Gervasini, J.A. Perdigon-Melon, C. Guimon, A. Auroux, *J. Phys. Chem. B* 110 (2006) 240–249.
- [23] K. Nakagawa, M. Okamura, N. Ikenaga, T. Suzuki, T. Kobayashi, *Chem. Commun.* 102 (1998) 5–1026.
- [24] S.E. Collins, M.A. Baltanas, A.L. Bonivardi, *J. Phys. Chem. B* 110 (2006) 5498–5507.
- [25] G. Aguilar-Rios, M. Valenzuela, P. Salas, H. Armendariz, P. Bosch, G. Del Toro, R. Silva, V. Bertin, S. Castillo, A. Ramirez-Solis, I. Schiffer, *Appl. Catal. A: Gen.* 127 (1995) 65–75.